Available at www.sciencedirect.com

INFORMATION PROCESSING IN AGRICULTURE 7 (2020) 20–29

journal homepage: www.elsevier.com/locate/inpa

Height stability control of a large sprayer body based on air suspension using the sliding mode approach

Yu Chen [a], Shuo Zhang [a], Enrong Mao [b], Yuefeng Du [b], Jun Chen [a,*], Shanju Yang [a]

[a] College of Mechanical and Electronic Engineering, Northwest A&F University, Yangling, Shaanxi 712100, China
[b] College of Engineering, China Agricultural University, Beijing 100083, China

ARTICLE INFO

Article history:
Received 16 January 2019
Received in revised form
14 May 2019
Accepted 12 June 2019
Available online 15 June 2019

Keywords:
Agricultural machinery
High clearance self-propelled sprayer
Sliding mode approach
Air suspension
Height stability control

ABSTRACT

When a high clearance self-propelled sprayer sprays, the sprung mass varies with the amount of liquid in the tank, which causes a change in the height of the sprayer body. This change not only is harmful to the sprayer ride comfort, but also has a greater impact on the sprayer application quality. In this paper, a large-scale high clearance self-propelled sprayer with air suspension was taken as the research object. Based on vehicle dynamics and air thermodynamics theory, a mathematical model of air spring inflation/deflation was established, then a 3 degree of freedom (3-dof) vertical dynamics model of sprayer air suspension was built. On this basis, the height control strategy of the sprayer body was formulated. Due to the nonlinear characteristics of air suspension, two control algorithms, namely sliding mode control and the on-off control, were used to design the suspension height stability controller, respectively. A simulation experiment was carried out by using the sprayer spraying crops as an example. The simulation experiment results showed that sliding mode control and on-off control could track and stabilize the height of the sprayer body when it changed under no excitation and D-grade road random excitation. However, due to strong nonlinearity and hysteresis of the pneumatic system, on-off control precision was poor. With the on-off control method, further reduction of the sprung mass would change the internal parameters of the pneumatic system, cause the air spring over deflation, even worse, the over deflation phenomenon presented a serious trend and cause system instability under random road excitation. Compared with on-off control method, sliding mode control approach had good control ability and precision due to its robustness to change in model parameters. The research will provide a reference for the height stability adjustment of large high clearance self-propelled sprayers during spraying and dosing operations.

1. Introduction

As an important machine for spraying and fertilizing crops, High clearance self-propelled sprayer is widely used for its

* Corresponding author at: Northwest A&F University, 3 Taicheng Road, Yangling, Shaanxi 712100, China.
E-mail address: chenjun_jdxy@nwafu.edu.cn (J. Chen).
Peer review under responsibility of China Agricultural University.
https://doi.org/10.1016/j.inpa.2019.06.003

high efficiency, environmental protection and intelligence [1,2]. The large-scale high clearance self-propelled sprayer has fast driving speed, high working efficiency, and sprung mass changes with the amount of liquid in the tank. It needs to be equipped with a special suspension system to meet some requirements, such as high ground clearance, large vibration reduction stroke, easy four-wheel steering and track adjustment requirements [3–5]. Because of good nonlinear elastic characteristics, large suspension stroke, adjustable load capacity, large bearing mass and low vibration frequency [6–10], air springs and hydro-pneumatic springs are widely used in sprayers [11-13]. For example, John Deere [14,15] and Hagie [16,17] are equipped with independent strut air suspension and body leveling systems, which can effectively cushion the impact of uneven ground and reduce the vibration of the spray bar when the sprayer passes through uneven ground. In addition, AGCO [18,19], AgriFac [20,21] and other sprayer companies have applied for patents on air suspension, and the new generation of sprayers are equipped with air suspension.

The operating conditions of the sprayer are complicated. To ensure the smooth operation of the sprayer and the quality of the spray to the greatest extent, scholars have conducted extensive research on it. Krohn designed a multichamber liquid tank water deflate control system to prevent the load distribution of the front and rear axles from changing the liquid quality of the liquid tank during the operation of the sprayer. The chambers sequentially deflate water according to the feedback signal of the liquid level sensor installed inside, and finally the center of gravity of the whole machine is always maintained within a certain range [22]. Čedík had shown through experimental studies that sprayers equipped with radial tires have better ride comfort and less soil compaction than ordinary bias tires [23]. Thmasebi proposed an active torque control method based on the boom suspension for the vibration of the sprayer boom caused by ground excitation. The neural network PID was used to control the boom suspension [24,25]. The results showed that the method could effectively suppress the vibration of the sprayer boom structure and had better shimmy suppression performance. These studies, however, have focused on analysis of characteristics and control of the sprayer boom suspension [26,27]; research on the stability control of the sprayer body has not been reported.

Traditional sprayer manufacturers use mechanical height control valves to adjust the height of the sprayer body. This passive adjustment method is simple and easy to implement and can better track the height of the vehicle. The disadvantage is that the body can only be maintained passively at a fixed height. When the tilting of the body during the operation of the sprayer causes the tire load to be unbalanced, it may cause a safety hazard. The combination of height sensor and solenoid valve to control the height of the vehicle is studied on road vehicles [28,29]. Sun et al. applied hybrid system theory to design a novel electronic suspension height control strategy. The simulation analysis and experimental research on the control strategy showed that the proposed control strategy could not only effectively adjust the height of the vehicle but also realize the direct control of the on-off state of the solenoid valve [30]. Kim et al. applied the sliding mode control method to the vehicle height control and level control for the strong nonlinearity and hysteresis of the air suspension [31,32]. Based on the electronically controlled air suspension, Xu et al. proposed a fuzzy variable structure control. The simulation results showed that the proposed control method could track the suspension height [33].

In summary, there are few studies on height stability control of large-scale high clearance self-propelled sprayers. The above research shows that the current domestic and international research has realized the application of electromagnetic valve to control the road vehicle body height, and the control effect is better, which can provide some references for the studied of the sprayer body height control. However, since the sprayer is an agricultural machine, the road conditions and operating conditions are quite different compared with road vehicles. During the spraying and dosing process of the sprayer, the mass of the sprung is changed at all times. If the vehicle body height control algorithm of the road vehicle is applied to the sprayer, the control result will not achieve the desired result. In this paper, the sprayer with air suspension is taken as the research object, and the variation law of the liquid quality in the tank under the spring and the dosing task is analyzed. Through an appropriate control strategy and algorithm, the height of the body of the sprayer is stabilized when the sprung mass changes.

2. Methods

2.1. Analysis of sprayer operating conditions

The sprung mass will change when the sprayer is spraying. For some small sprayers and spray emasculation machines, due to the limited capacity of the liquid tank, this change is distributed to each spring without causing a wide range of fluctuations in the height of sprayer body, so there is no need to install adjustment devices to maintain the stability of the body. However, as shown in Fig. 1, for a large self-propelled sprayer, the capacity of the liquid tank is 4000–12,000 L. From no load to full load, it will cause a wide range of changes in the body height, and appropriate adjustment devices and control strategies are needed to offset the impact of load changes on the body height. H_1, H_2, and H_3 are the heights of the sprayer body under the different liquid quality in the Figure, and the unit is m. Among them, $H_1 > H_2 > H_3$.

2.2. Mathematical model

2.2.1. Analysis model of suspension height adjustment process

The air suspension height adjustment of the sprayer based on inflation/deflation of air spring. Fig. 2 shows a schematic diagram of the air flow during the adjustment of the air suspension height. The solid line in the Figure is the air spring height lifting process, and the broken line is the height lowering process. During the sprayer spraying process, the mass of the sprayer body changes with the quality of the liquid in the tank. The air spring is deformed under the load of the body and its internal air pressure, so that the height sensor's swinging rod mounted on the upper and lower sides of the spring, swings synchronously. The electronic control unit

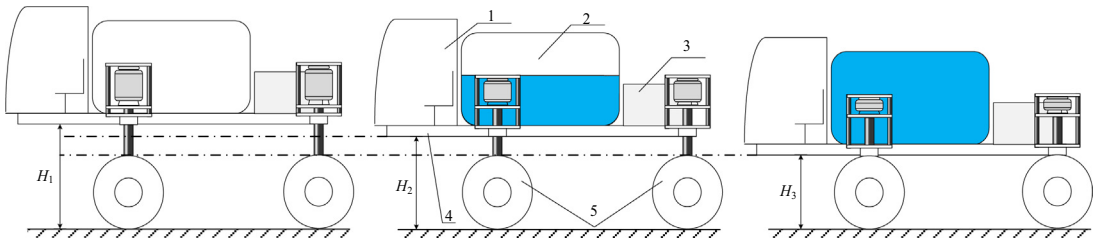

(a) empty (b) one half (c) fill

1-cab; 2-liquid tank; 3-engine; 4-frame; 5-pneumatic suspension

Fig. 1 – Schematic diagram of the sprayer's body height changing with reagent liquid dosage.

(ECU) in the controller compares the real-time electrical pulse signal measured by the sensor with the initial signal and converts the difference between the current vehicle height and the target vehicle height into an electrical pulse signal and transmits it to the three-position three-way solenoid valve. The electric pulse signal determines whether the solenoid valve spool is in the upper position (aeration) or the lower position (exhaust). The pulse length determines the spool position duration, then to achieve height control of the sprayer body by controlling the amount of spring gas inflated or the amount of spring gas deflated.

Since the height adjustment process of the sprayer suspension has strong nonlinearity, the arrangement and composition of the gas circuit between the gasholder and the air spring should be fully considered. Combining the thermodynamic law of variable mass gas with the internal gas state of the spring and the dynamic behavior of the sprung mass when the suspension height is adjusted, a suspension height adjustment analysis model is established using the modeling process of [6,8], as shown in Eqs. (1) and (2), to achieve a nonlinear description of the adjustment process. The established model provides the basis for the next step of air suspension height control.

$$\text{When the spring is inflated}\begin{cases} G_c = \frac{c_d K p_c A_{K1} N_c}{\sqrt{T_c}} \\ \dot{p}_c = -\frac{nRT_{c0}}{V}\left(\frac{p_c}{p_{c0}}\right)^{\frac{n-1}{n}} G_c \\ \dot{p}_1 = -\frac{np_1}{V_1}\dot{V}_1 + \frac{nRT_{10}}{V_1}\left(\frac{p_1}{p_{10}}\right)^{\frac{n-1}{n}} G_c \\ m_b(\ddot{x}_b + g) + c_s(\dot{x}_b - \dot{x}_t) = (p_1 - p_a)A_e \end{cases} \quad (1)$$

$$\text{When the spring is deflated}\begin{cases} G_k = -\frac{c_d K p_1 A_{K1} N_k}{\sqrt{T_1}} \\ \dot{p}_1 = -\frac{np_1}{V_1}\dot{V}_1 - \frac{nRT_{10}}{V_1}\left(\frac{p_1}{p_{10}}\right)^{\frac{n-1}{n}} G_k \\ m_b(\ddot{x}_b + g) + c_s(\dot{x}_b - \dot{x}_t) = (p_1 - p_a)A_e \end{cases} \quad (2)$$

In formulas (1) and (2), p_c is the absolute pressure in the gasholder during the inflation process of air spring, MPa; T_{c0} (K) and p_{c0} (MPa) are the initial gas temperature and absolute pressure in the gasholder, respectively; V is the gasholder volume, m^3; n is the gas adiabatic index, 1.4; R is the gas constant, 287.1 J/(kg·K); c_d is the throttle valve shrinkage coefficient, 0.62; A_{k1} is the solenoid valve port area, m^2; T_c and T_1 are the gas temperature in the gasholder and air spring, respectively, K; p_1 is the absolute pressure in the air spring, MPa; p_a is the atmospheric pressure, 0.1 MPa; m_b is the sprung mass, kg; g is gravity acceleration, 9.8 m/s^2; C_s is the suspension damping force, N·s/m; x_b and x_t are the sprung mass and unsprung mass displacement, respectively, m; A_e is the effective cross-sectional area of the air spring, m^2; T_{10} (K) and p_{10} (MPa) are the initial gas temperature and absolute pressure in the air spring, respectively; and V_1 is the air spring volume, m^3.

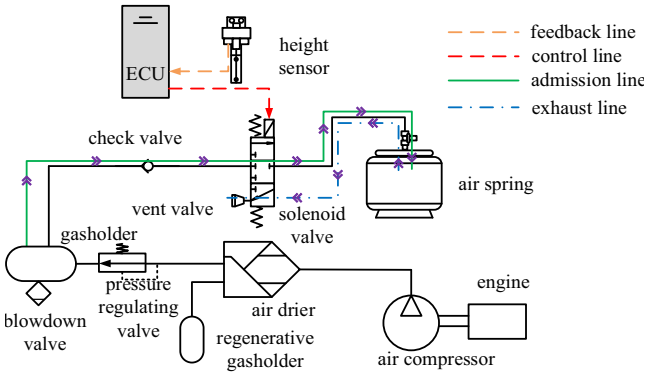

Fig. 2 – Air flow diagram of the air suspension height adjustment process.

2.2.2. 3-dof dynamics model of sprayer

Assuming that the body and liquid tank of the sprayer are rigid, if the tire load transfer caused by the vehicle altitude is not considered, then the road surface irregularity and the vertical dynamics of the tire are temporarily ignored. When the sprayer is running at a constant speed on a horizontal road surface, the 3-dof dynamic model of the sprayer is established, as shown in Fig. 3.

In Fig. 3, θ and φ are the roll angle and the pitch angle of the sprayer body in the inertial reference frame ***In*** respectively, rad; ω_x and ω_y are the rotational angular velocities of the m-axis and the n-axis of the center mass around the body coordinate system ***CoG,*** respectively, that is, the body roll and pitch angular velocity, rad/s; v is the sprayer travel speed, m/s; m_s is the sprung mass, kg; B_F is the wheel track, m; a and b are

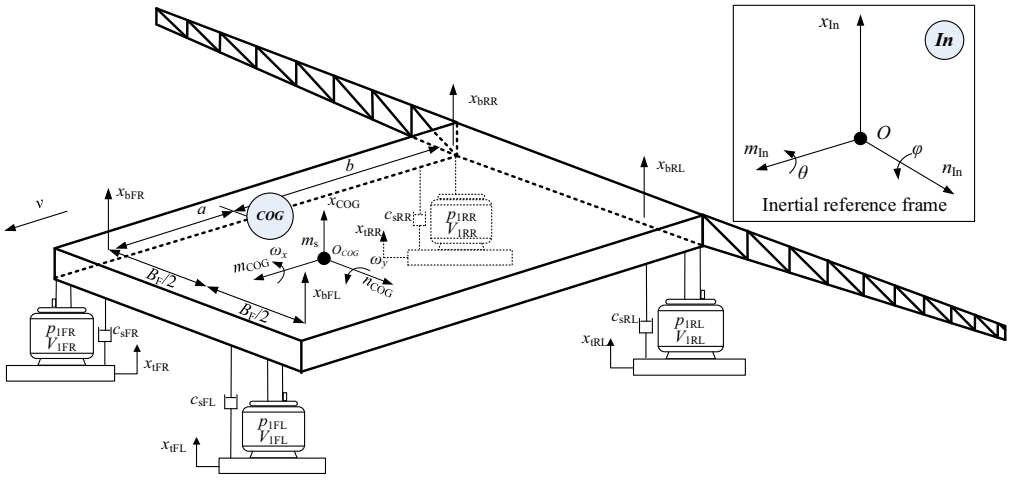

Fig. 3 – 3-dof freedom nonlinear model of sprayer air suspension.

the projection distance of the center of mass to the front and rear axles on the ground, respectively, m; x_{COG} is the vertical displacement at the center of mass of the vehicle, m; x_{bij} is the four-spindle sprung mass displacement, m; x_{tij} is the road excitation input of four wheels, respectively, m; c_{sij} is four suspension damping, N·s/m; and p_{1ij} (MPa) and V_{1ij} (m^3) are the internal spring pressure and volume of the four suspensions, respectively. The index ij takes the values FL, FR, RL, and RR to indicate the four suspension positions of the entire machine. If the moment of inertia of the sprung mass roll and pitch are J_r, J_p, respectively (unit: kg·m^2), the sprung mass centroid to the roll and pitch center distance are h_r, h_p (unit: m), respectively. According to Newton's second law, combined with formulas (1) and (2), the mathematical model of the whole process of the sprayer stabilization process is shown in Eq. (3).

$$\begin{cases} \dot{p}_{1ij} = -\frac{np_{1ij}A_{eij}\dot{x}_{ij}}{V_{1ij}} + \frac{nRT_{1ij}}{V_{1ij}}\left(\frac{p_{1ij}}{p_{10ij}}\right)^{\frac{n-1}{n}}u_{ij} \\ \ddot{x}_{COG} = \frac{1}{m_s}\left(\sum\left(\left(p_{1ij}-p_a\right)A_{eij} - c_{dij}\dot{x}_{ij}\right) - m_s g\right) \\ \ddot{\theta} = \frac{B_F}{2J_r}\begin{pmatrix} (p_{1FL}-p_a)A_{eFL} - (p_{1FR}-p_a)A_{eFR} \\ +(p_{1RL}-p_a)A_{eRL} - (p_{1RR}-p_a)A_{eRR} \\ -c_{sFL}\dot{x}_{FL} + c_{sFR}\dot{x}_{FR} - c_{sRL}\dot{x}_{RL} + c_{sRR}\dot{x}_{RR} \end{pmatrix} \\ \ddot{\varphi} = \frac{1}{J_p}\begin{pmatrix} b((p_{1RL}-p_a)A_{eRL} + (p_{1RR}-p_a)A_{eRR}) \\ -a((p_{1FL}-p_a)A_{eFL} + (p_{1FR}-p_a)A_{eFR}) \\ +a(c_{sFL}\dot{x}_{FL} + c_{sFR}\dot{x}_{FR}) - b(c_{sRL}\dot{x}_{RL} + c_{sRR}\dot{x}_{RR}) \end{pmatrix} \\ V_{1ij} = A_{eij}\left(x_{0ij} + x_{ij}\right) \\ x_{ij} = x_{bij} - x_{tij} \end{cases} \tag{3}$$

In formula (3), u_{ij} is the control amount, x_{ij} is the air spring dynamic displacement, and x_{0ij} is the height when the air spring is in the equilibrium position. x_{bij} can be expressed by the sprayer body roll angle θ, the pitch angle φ and the vertical displacement x_{COG} at the center of mass:

$$\begin{cases} x_{bFL} = x_{COG} + \frac{B_F}{2}\theta - a\varphi \\ x_{bFR} = x_{COG} - \frac{B_F}{2}\theta - a\varphi \\ x_{bRL} = x_{COG} + \frac{B_F}{2}\theta + b\varphi \\ x_{bRR} = x_{COG} - \frac{B_F}{2}\theta + b\varphi \end{cases} \tag{4}$$

2.3. *Controller design*

2.3.1. *Control strategy*

Fig. 4 shows the height adjustment strategy of the sprayer body during the time-varying process of the sprung mass. In the initial state, the sprayer suspension is maintained at the initial height and remains unchanged. When the dosing or spraying is started, the increase or decrease of the sprung mass will cause the change of the height of the sprayer body. The height sensor records the change process in real time and transmits the collected height signal to the controller. When the amount of altitude change exceeds a set threshold, the controller controls the solenoid valve to inflate or deflate air

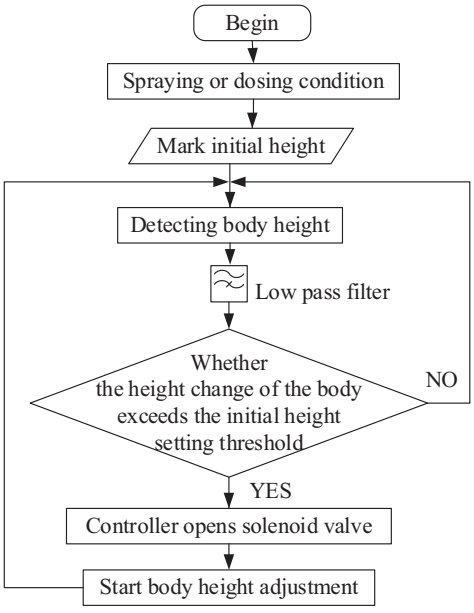

Fig. 4 – Ride height adjustment strategy of sprung mass time-varying process.

spring until the air spring returns to the initial height. For the height signal measured by the sensor, the low-pass filter of 0.01 Hz can filter out the change in the body displacement caused by the unsprung mass and other vibration factors, thereby obtaining the vehicle body height change signal caused only by the sprung mass change.

2.3.2. *Control algorithm*

The height stability control of the sprayer body is mainly for the sprayer under dosing/spraying conditions. When the height of the sprayer body changes, the air suspension is inflated/deflated to maintain the height value within a fixed range to guarantee spray quality and ride comfort of the sprayer. Due to the strong nonlinearity and hysteresis of the air suspension, coupled with the time-varying and sprung mass uncertainty of the large sprayer during dosing/spraying, the traditional mechanical height control valve cannot accurately adjust the body height. Aiming at solving this problem, this paper designs a sprayer body height stabilization algorithm based on sliding mode control, as shown in Fig. 5. The real-time sprayer body height x_{COG}, roll angle θ, and pitch angle φ are obtained by the suspension model and the vertical dynamics model of the whole machine, and these values are compared with the target values. Then, the air inflate/deflate amount of each air suspension is obtained by the sliding mode controller and ultimately stabilizes the sprayer body height value within the target range.

2.3.3. *Establishment of sprayer body height stability control model*

According to formulas (3) and (4) and diagrams (4) and (5), in the sprayer body stability control process, the control amounts u_{ij} of the four three-position three-way solenoid valves can be equivalently calculated by the roll angle u_θ, the pitch angle control amount u_φ and the vertical displacement control quantity u_{xCOG} at the center of mass of the whole machine, as shown in formula (5).

$$\begin{cases} u_{FL} = u_\theta - u_\varphi + u_{xCOG} \\ u_{FR} = -u_\theta - u_\varphi + u_{xCOG} \\ u_{RL} = u_\theta + u_\varphi + u_{xCOG} \\ u_{RR} = -u_\theta + u_\varphi + u_{xCOG} \end{cases} \tag{5}$$

Applying the equivalent control quantities u_θ, u_φ and u_{xCOG}, the sprayer body height stability control model can be expressed as a state equation as shown in Eq. (6).

$$\begin{cases} \dot{x} = f(x) + g(x)u \\ x = [x_{COG} \quad \dot{x}_{COG} \quad \theta \quad \dot{\theta} \quad \varphi \quad \dot{\varphi} \quad p_{1FL} \quad p_{1FR} \quad p_{1RL} \quad p_{1RR}]^T \\ u = [u_{xCOG} \quad u_\theta \quad u_\varphi]^T \\ y = [x_{COG} \quad \theta \quad \varphi]^T \end{cases} \tag{6}$$

For 4 same type air springs mounted on the sprayer, it meets:

$$A_{eFL} = A_{eFR} = A_{eRL} = A_{eRR} = A_e \tag{7}$$

It can be determined from the model of the height control of the sprayer of the formula (3)–(6) that the height adjustment process is a nonlinear process. For the design of the sliding mode controller, the model needs to be linearized locally. Define new state variables

$$\begin{aligned} \vartheta &= [\vartheta_1 \quad \vartheta_2 \quad \vartheta_3 \quad \vartheta_4 \quad \vartheta_5 \quad \vartheta_6 \quad \vartheta_7 \quad \vartheta_8 \quad \vartheta_9]^T \\ &= [x_{COG} \quad f_1 \quad f_2 \quad \theta \quad f_3 \quad f_4 \quad \varphi \quad f_5 \quad f_6]^T \end{aligned} \tag{8}$$

According to the feedback linearization theory, the nonlinear system Eq. (6) is transformed into a state equation in linear space.

$$\begin{cases} \dot{\vartheta} = \begin{bmatrix} 0 & 1 & 0 & 0 & 0 & 0 & 0 & 0 & 0 \\ 0 & 0 & 1 & 0 & 0 & 0 & 0 & 0 & 0 \\ 0 & 0 & 0 & 0 & 0 & 0 & 0 & 0 & 0 \\ 0 & 0 & 0 & 0 & 1 & 0 & 0 & 0 & 0 \\ 0 & 0 & 0 & 0 & 0 & 1 & 0 & 0 & 0 \\ 0 & 0 & 0 & 0 & 0 & 0 & 0 & 0 & 0 \\ 0 & 0 & 0 & 0 & 0 & 0 & 0 & 1 & 0 \\ 0 & 0 & 0 & 0 & 0 & 0 & 0 & 0 & 1 \\ 0 & 0 & 0 & 0 & 0 & 0 & 0 & 0 & 0 \end{bmatrix} \vartheta + \begin{bmatrix} 0 & 0 & 0 \\ 0 & 0 & 0 \\ 1 & 0 & 0 \\ 0 & 0 & 0 \\ 0 & 0 & 0 \\ 0 & 1 & 0 \\ 0 & 0 & 0 \\ 0 & 0 & 0 \\ 0 & 0 & 1 \end{bmatrix} \upsilon \\ y = [\vartheta_1 \quad \vartheta_4 \quad \vartheta_7]^T \end{cases} \tag{9}$$

Wherein, υ is the control quantity of the linear system in the new coordinate system, and the relationship between υ and the original control quantity $\boldsymbol{u}$ is expressed in Eq. (10).

$$\upsilon = \begin{bmatrix} \upsilon_1 \\ \upsilon_2 \\ \upsilon_3 \end{bmatrix} = \begin{bmatrix} L_f{}^3 h_1(x) \\ L_f{}^3 h_2(x) \\ L_f{}^3 h_3(x) \end{bmatrix} + \begin{bmatrix} L_{g1} L_f{}^2 h_1(x) & L_{g2} L_f{}^2 h_1(x) & L_{g3} L_f{}^2 h_1(x) \\ L_{g1} L_f{}^2 h_2(x) & L_{g2} L_f{}^2 h_2(x) & L_{g3} L_f{}^2 h_2(x) \\ L_{g1} L_f{}^2 h_3(x) & L_{g2} L_f{}^2 h_3(x) & L_{g3} L_f{}^2 h_3(x) \end{bmatrix} \mathbf{u} \tag{10}$$

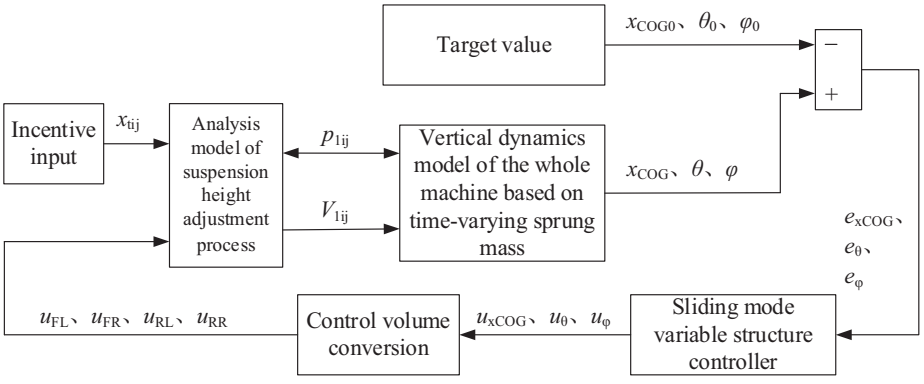

Fig. 5 – The control algorithm of ride height stabilization.

Through the transformation relationship of Eq. (10), if the system control quantity υ under the linear system is known, then the control quantity u under the sprayer body height adjustment system can be obtained by inverse coordinate transformation.

2.3.4. Design of the sliding mode controller

For a linearized sprayer body height adjustment system, define the output error as:

$$\begin{cases} e_{xCOG} = \vartheta_1 - \vartheta_{d1} \\ e_\theta = \vartheta_4 - \vartheta_{d4} \\ e_\varphi = \vartheta_7 - \vartheta_{d7} \end{cases} \tag{11}$$

In formula (11), ϑ_{d1}, ϑ_{d4}, and ϑ_{d7} are the target sprayer body height, the body roll angle, and the pitch angle, respectively. Using sliding mode variable structure control, the control sliding surface of the body height, body roll angle and pitch angle can be designed as:

$$\begin{cases} s_{xCOG} = \lambda_{xCOG}^2 e_{xCOG} + 2\lambda_{xCOG}\dot{e}_{xCOG} + \ddot{e}_{xCOG} \\ s_\theta = \lambda_\theta^2 e_\theta + 2\lambda_\theta \dot{e}_\theta + \ddot{e}_\theta \\ s_\varphi = \lambda_\varphi^2 e_\varphi + 2\lambda_\varphi \dot{e}_\varphi + \ddot{e}_\varphi \end{cases} \tag{12}$$

Wherein, λ_x, λ_θ and λ_φ are slip mode coefficients, and both are greater than zero. For different sliding mode control quantities, the Lyapunov function $V(s_n) = s_n^2/2$ is designed. According to the Lyapunov stability theory, if the designed control system is stable, then Eq. (13) must be satisfied. Where η_n is an arbitrarily small positive integer and n represents a different sliding surface identifier that is x_{COG}, θ and φ.

$$\dot{V}(s_n) = \frac{1}{2}\frac{d}{dt}s_n^2 = s_n\dot{s}_n \leqslant -\eta_n|s_n| \tag{13}$$

In formula (13), s_n can be obtained from formula (12). $\dot{s}_n$ can be obtained by combining the derivative of formula (12) with formula (9), as shown in formula (14).

$$\begin{bmatrix} \dot{s}_{xCOG} \\ \dot{s}_\theta \\ \dot{s}_\varphi \end{bmatrix} = \begin{bmatrix} \lambda_{xCOG}^2\dot{e}_{xCOG} + 2\lambda_{xCOG}\ddot{e}_{xCOG} - \dddot{\vartheta}_{d1} \\ \lambda_\theta^2\dot{e}_\theta + 2\lambda_\theta\ddot{e}_\theta - \dddot{\vartheta}_{d4} \\ \lambda_\varphi^2\dot{e}_\varphi + 2\lambda_\varphi\ddot{e}_\varphi - \dddot{\vartheta}_{d7} \end{bmatrix} + \begin{bmatrix} \upsilon_1 \\ \upsilon_2 \\ \upsilon_3 \end{bmatrix} \tag{14}$$

Assuming that the system dynamic error is in the sliding mode plane, then $s = \dot{s} = 0$, the control amount of the original height adjustment system can be obtained according to Eqs. (10) and (14) as shown in Eq. (15). In formula (15), the on-off control is adopted, that is, a discontinuity is added, so that the system still has better dynamic quality under the condition of large disturbance and sway, wherein ε_{xCOG}, ε_θ, ε_φ are all greater than zero.

$$\begin{bmatrix} \upsilon_1 \\ \upsilon_2 \\ \upsilon_3 \end{bmatrix} = \begin{bmatrix} -\lambda_{xCOG}^2\dot{e}_{xCOG} - 2\lambda_{xCOG}\ddot{e}_{xCOG} + \dddot{\vartheta}_{d1} \\ -\lambda_\theta^2\dot{e}_\theta - 2\lambda_\theta\ddot{e}_\theta + \dddot{\vartheta}_{d4} \\ -\lambda_\varphi^2\dot{e}_\varphi - 2\lambda_\varphi\ddot{e}_\varphi + \dddot{\vartheta}_{d7} \end{bmatrix} - \begin{bmatrix} \varepsilon_{xCOG}sgn(s_{xCOG}) \\ \varepsilon_\theta sgn(s_\theta) \\ \varepsilon_\varphi sgn(s_\varphi) \end{bmatrix} \tag{15}$$

Bringing Eq. (15) into Eq. (14):

$$\begin{bmatrix} \dot{s}_{xCOG} \\ \dot{s}_\theta \\ \dot{s}_\varphi \end{bmatrix} = -\begin{bmatrix} \varepsilon_{xCOG}sgn(s_{xCOG}) \\ \varepsilon_\theta sgn(s_\theta) \\ \varepsilon_\varphi sgn(s_\varphi) \end{bmatrix} \tag{16}$$

That is

$$\begin{aligned} s_n\dot{s}_n &= \begin{bmatrix} s_{xCOG} \\ s_\theta \\ s_\varphi \end{bmatrix}\begin{bmatrix} \dot{s}_{xCOG} \\ \dot{s}_\theta \\ \dot{s}_\varphi \end{bmatrix} = \begin{bmatrix} s_{xCOG} \\ s_\theta \\ s_\varphi \end{bmatrix}\begin{bmatrix} -\varepsilon_{xCOG}sgn(s_{xCOG}) \\ -\varepsilon_\theta sgn(s_\theta) \\ -\varepsilon_\varphi sgn(s_\varphi) \end{bmatrix} \\ &\leqslant \begin{bmatrix} -\eta_{xCOG} \\ -\eta_\theta \\ -\eta_\varphi \end{bmatrix} \times \left|\begin{bmatrix} s_{xCOG} \\ s_\theta \\ s_\varphi \end{bmatrix}\right| \end{aligned} \tag{17}$$

According to Eq. (17), if $\varepsilon_{xCOG} \geq \eta_{xCOG}$, $\varepsilon_\theta \geq \eta_\theta$, $\varepsilon_\varphi \geq \eta_\varphi$ are satisfied, then the control system in the new coordinates is stable. To reduce the system "chattering" caused by the error in the model construction, the continuous saturation function $sat(s/\psi)$ is used instead of the on-off term in Eq. (15), and the control system control quantity expression is obtained as Eq. (18) shows.

$$\begin{bmatrix} \upsilon_1 \\ \upsilon_2 \\ \upsilon_3 \end{bmatrix} = \begin{bmatrix} -\lambda_{xCOG}^2\dot{e}_{xCOG} - 2\lambda_{xCOG}\ddot{e}_{xCOG} + \dddot{\vartheta}_{d1} \\ -\lambda_\theta^2\dot{e}_\theta - 2\lambda_\theta\ddot{e}_\theta + \dddot{\vartheta}_{d4} \\ -\lambda_\varphi^2\dot{e}_\varphi - 2\lambda_\varphi\ddot{e}_\varphi + \dddot{\vartheta}_{d7} \end{bmatrix} - \begin{bmatrix} \varepsilon_{xCOG}sat(s_{xCOG}/\psi_{xCOG}) \\ \varepsilon_\theta sat(s_\theta/\psi_\theta) \\ \varepsilon_\varphi sat(s_\varphi/\psi_\varphi) \end{bmatrix} \tag{18}$$

Bringing Eq. (18) into Eq. (10), the nonlinear system control is:

$$\begin{aligned} \begin{bmatrix} u_{xCOG} \\ u_\theta \\ u_\varphi \end{bmatrix} = &\begin{bmatrix} L_{g1}L_f{}^2h_1(x) & L_{g2}L_f{}^2h_1(x) & L_{g3}L_f{}^2h_1(x) \\ L_{g1}L_f{}^2h_2(x) & L_{g2}L_f{}^2h_2(x) & L_{g3}L_f{}^2h_2(x) \\ L_{g1}L_f{}^2h_3(x) & L_{g2}L_f{}^2h_3(x) & L_{g3}L_f{}^2h_3(x) \end{bmatrix}^{-1} \\ &\times \left(\begin{bmatrix} -\lambda_{xCOG}^2\dot{e}_{xCOG} - 2\lambda_{xCOG}\ddot{e}_{xCOG} + \dddot{\vartheta}_{d1} - L_f{}^3h_1(x) \\ -\lambda_\theta^2\dot{e}_\theta - 2\lambda_\theta\ddot{e}_\theta + \dddot{\vartheta}_{d4} - L_f^3h_2(x) \\ -\lambda_\varphi^2\dot{e}_\varphi - 2\lambda_\varphi\ddot{e}_\varphi + \dddot{\vartheta}_{d7} - L_f^3h_3(x) \end{bmatrix} \right. \\ &\left. - \begin{bmatrix} \varepsilon_{xCOG}sat(s_{xCOG}/\psi_{xCOG}) \\ \varepsilon_\theta sat(s_\theta/\psi_\theta) \\ \varepsilon_\varphi sat(s_\varphi/\psi_\varphi) \end{bmatrix} \right) \end{aligned} \tag{19}$$

From formula (19) and formula (5), the control flow rate u_{ij} through the solenoid valve during the height control of the sprayer can be obtained and the actual solenoid valve can be controlled by the pulse width modulation (PWM) method. The actual on-off state duty cycle of the solenoid valve can be obtained from Eq. (20).

$$u_{ijPWM} = \begin{cases} 1 & \text{if } u_{ij} \geqslant |u_{0max}| \\ u_{ij}/|u_{0max}| & \text{if } 0 < u_{ij} < |u_{0max}| \\ 0 & \text{if } u_{ij} \leqslant 0 \end{cases} \tag{20}$$

In Eq. (20), u_{ijPWM} is the duty cycle of the solenoid valve's actual on-off state; u_{0max} is the product of the air mass flow rate and the unit control period when the solenoid valve is fully opened. By formula (20), the mass flow value required for the height control process can be converted into the duty ratio in the electromagnetic signal of the solenoid valve on-off, thereby making it easier to control the solenoid valve. u_{0max} can be obtained by Eq. (21).

$$u_{0maxij} = \begin{cases} c_d K A_{K1} p_c N_c/\sqrt{T_c} & \text{When the sprayer refills} \\ -c_d K A_{K1} p_{1ij} N_k/\sqrt{T_1} & \text{When the sprayer sprays} \end{cases} \tag{21}$$

3. Results and discussion

MATLAB/Simulink was used to establish the simulation model of the air suspension height control system. The simulation time interval was set as 0.001 s and the simulation time was 1000 s. Other specific simulation parameters were shown in Table 1.

On-off control was equivalent to the control process of the mechanical body height valve on traditional sprayers. To verify the effect of the sliding mode control algorithm designed in this paper on the sprayer body height stability during the spraying operation, two kinds of excitation signals [34,35], namely, no excitation and D level road excitation, were adopted, respectively. The body height change, body roll angle change and body pitch angle change were selected as the evaluation indicators of control performance. At the same time, the control effect of the on-off was compared and analyzed. The simulation results were shown in Figs. 6–8.

Fig. 6 showed the control effect of sprayer body height stability with changing the sprayer body quality and without

Table 1 – Initial simulation parameters of vehicle stability control.

Parameters/unit	Instructions	Values	Parameters/unit	Instructions	Values
m_s/kg	Initial body mass	12,000	λ_θ	Sliding mode coefficient of body roll	7.235
J_r/kg·m^2	Roll moment of inertia	27812.5	λ_φ	Sliding mode coefficient of body pitch	19.351
J_p/kg·m^2	Pitch moment of inertia	20612.5	ε_{xCOG}	Switching constant of body height	1
B_F/m	Wheel track	3.2	ε_θ	Switching constant of body roll	1
a/m	Front axle distance from center of mass	1.8	ε_φ	Switching constant of body pitch	3
b/m	Rear axle distance from center of mass	2.2	ψ_{xCOG}	Boundary thickness of body height	0.01
v/km·h^{-1}	Speed	12	ψ_θ	Boundary thickness of body roll	0.01
λ_{xCOG}	Sliding mode coefficient of body height	10.134	ψ_φ	Boundary thickness of body pitch	0.01
x_{0ij}/mm	Initial spring height	380	V_{10ij}/m^3	The initial working volume of the spring	0.01914
V_1'	Rate of change in volume of the spring	0.518	T_{ij}/K	Internal spring temperature	293
C_{sij}/N·s·m^{-1}	Suspension damping	6475			

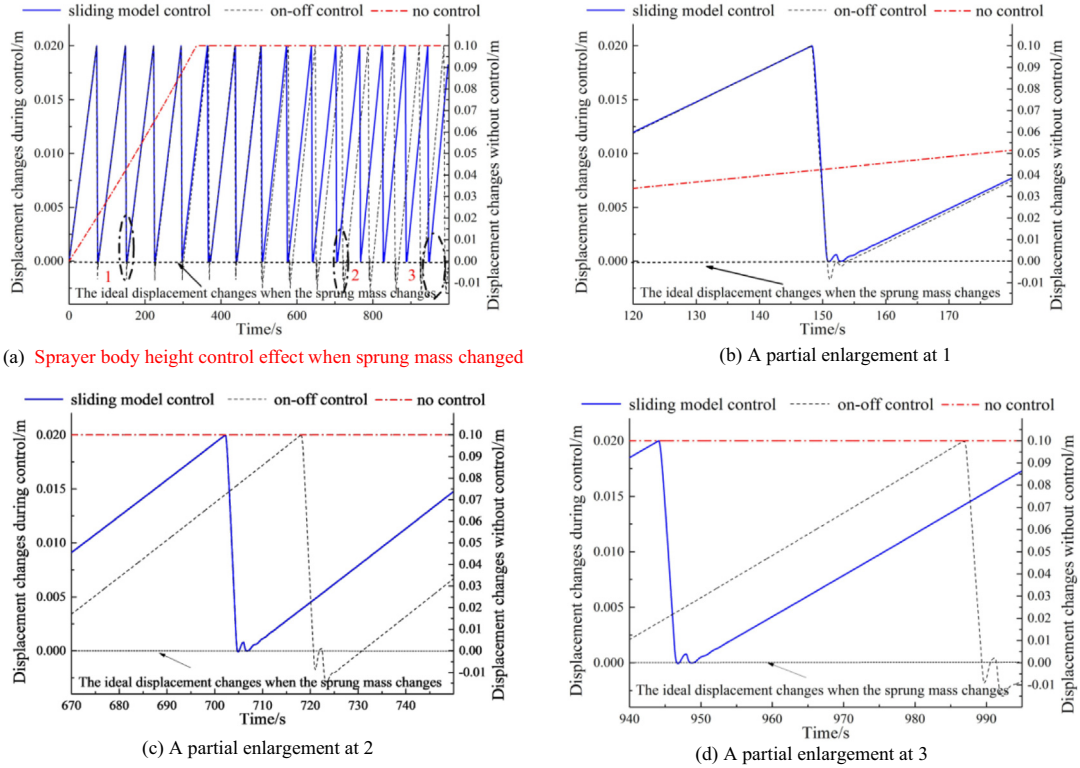

(a) Sprayer body height control effect when sprung mass changed

(b) A partial enlargement at 1

(c) A partial enlargement at 2

(d) A partial enlargement at 3

Fig. 6 – Ride height adjustment effect of sprung mass time-varying process (no excitation).

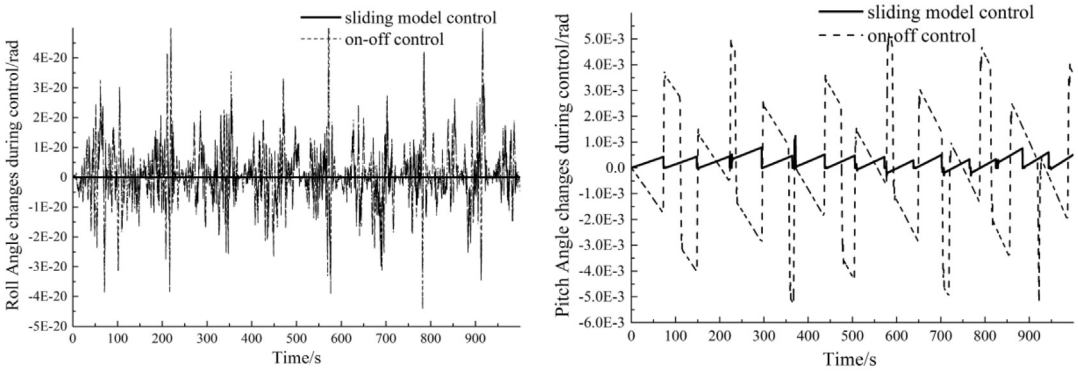

(a) Change in roll angle (b) Change in pitch angle

Fig. 7 – Variation tendency of roll angle and pitch angle (no excitation).

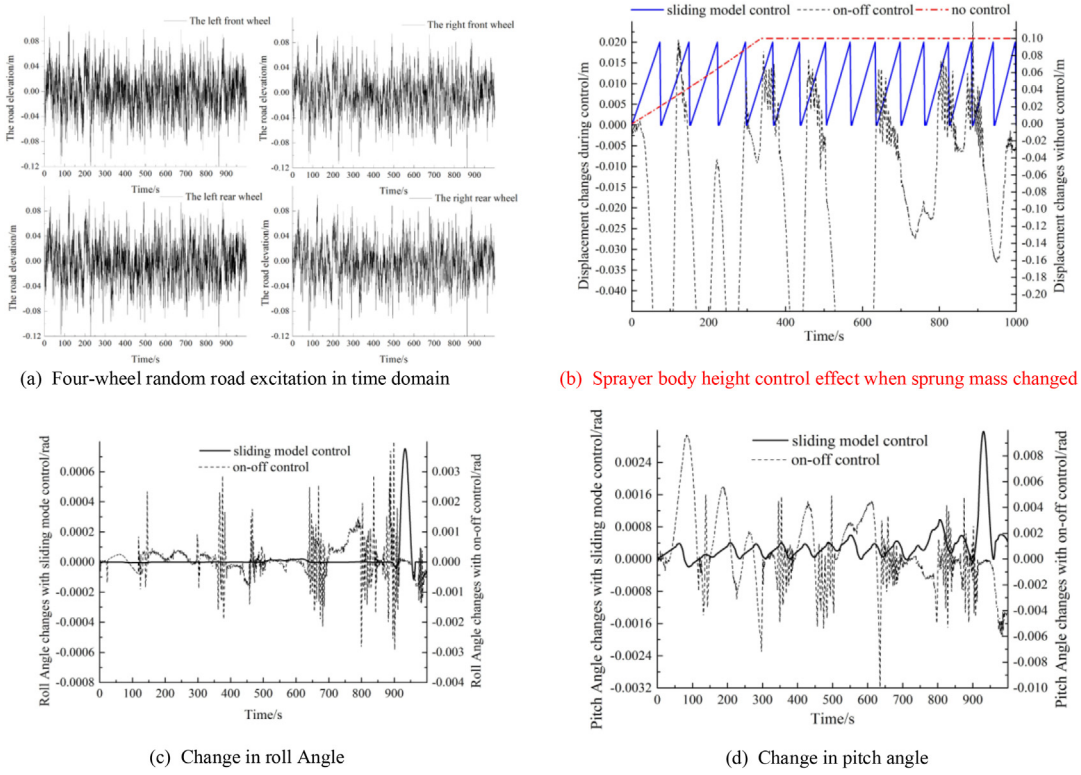

(a) Four-wheel random road excitation in time domain

(b) Sprayer body height control effect when sprung mass changed

(c) Change in roll Angle

(d) Change in pitch angle

Fig. 8 – Comparison of sliding model control and on-off control (D-grade road random excitation).

excitation. Take the reduction of body mass as an example (simulating the spray condition), without control, the air spring would be stretched under the action of internal gas pressure and thus increased the body height as shown in the dotted line in Fig. 6. After the body height increased by 0.1 m, the value would no longer change due to the effect of the limit block.

When on–off control was adopted (the dotted line in Fig. 6), due to the strong nonlinearity and hysteresis of the air circuit system, the system would overshoot due to excessive deflation of air. As shown in Fig. 6b–d, the overshoot at 1, 2, and 3 was about 0.002 m, 0.003 m, and 0.004 m. The reduction of the body quality caused internal parameters of suspension system to change, and the phenomenon of excessive deflating presented a serious trend. When sliding mode control was adopted (the solid line in Fig. 6), there was no overshoot. The sliding mode controller had high control precision. In addition, comparing the solid and dotted lines in Fig. 6b–d, the sliding mode control allowed the body height to reach the target height at 151 s, 705 s and 946 s. While the on-off control allowed the body height to reach the target height at 151 s, 720 s and 989 s. Sliding mode control had faster response and better control effect than on-off control.

Fig. 7a and b showed the changes of body's pitch angle and roll angle with two control algorithms during stabilized the sprayer body height. Compared with on-off control, when

sliding mode control was adopted, sprayer body's roll angle and pitch angle value were much smaller. The whole simulation process showed that the sliding mode control algorithm had good control effect and was more robustness with regard to changing model parameters. The sprayer had better smoothness in the process of body height stability using the sliding mode approach.

Fig. 8 showed the comparison of the effect of sliding mode control and on-off control on body stability control when the sprayer sprayed at the operating speed of 12 km/h under the excitation of the D-grade road random excitation. As shown in Fig. 8b, when on-off control was adopted, the height of the sprayer body could not be stabilized due to the interference of the ground excitation, and the whole system was in an unstable state. Since sliding mode control had good robustness to the variation of the model parameters, it was not affected by the ground excitation and had better anti-interference ability and higher control precision. Fig. 8a and b showed the changes of body's pitch angle and roll angle with two control algorithms during stabilized the sprayer body height under D-grade road random excitation. Compared with on-off control, when sliding mode control was adopted, sprayer body's roll angle and pitch angle value were much smaller. Through the simulation results of no road excitation and D-grade road random excitation, it was known that the body height stability algorithm designed in this paper based on sliding mode control had a good control effect.

4. Conclusions and future works

During the operation of the sprayer, a change in the amount of liquid leads to a change in the sprayer body height, which has an important impact on the sprayer's ride comfort and application effect. Therefore, stabilizing the sprayer body height is a key technology for the sprayer. Through this study, the following conclusions can be drawn:

(1) An analysis model of suspension height adjustment process and a 3-dof mathematical model of the sprayer are established in this paper, which comprehensively describe the vertical force of the sprayer and the change process of the spring height under spraying and dosing conditions, laying a theoretical foundation for sprayer body height stability control.
(2) The control strategy developed in this paper meets the needs of sprayer body height stability control and can provide a reference for the body height stability adjustment of large high clearance self-propelled sprayers.
(3) Compared with on-off control, the sliding mode variable structure sprayer control algorithm proposed in this paper is more robust and has better control response and precision to the change of model parameters. At the same time, while stabilizing the height of the body, the values of the body roll angle and pitch angle are small; therefore, the sprayer is smoother in the process of height stabilization.

The large scale high clearance self-developed sprayer trial production has been completed. Since the whole electrical control system is still in the commissioning stage. In the future, field experiment will be carried out to verify the proposed sprayer body height control algorithm.

Declaration of Competing Interest

The authors declared that there is no conflict of interest.

Acknowledgment

The authors thank the editing team of American Journal Experts for improving the English language fluency of our paper. The work in this paper was supported by the China Postdoctoral Science Foundation (No. 2018M643744) and the National Key Research and Development Program (No. 2018YFD0701100-2018YFD0701102).

REFERENCES

[1] Baumhardt UB, Airton DSA, Tenório HGT, Ferreira CC, Bedin PR. Methodology for conception of cabins of agricultural machines: informational phase applied to a self-propelled sprayer. J Braz Soc Mech Sci Eng 2017;39(5):1683–94.
[2] Julián S, Víctor JR, Francisco P, Francisco A, Carvajal F. Field evaluation of a self-propelled sprayer and effects of the application rate on spray deposition and losses to the ground in greenhouse tomato crops. Pest Manag Sci 2011;67(8):942–7.
[3] Anthonis J, Audenaert J, Ramon H. Design optimisation for the vertical suspension of a crop sprayer boom. Biosyst Eng 2005;90(2):153–60.
[4] Lardoux Y, Sinfort C, Enfalt P, Sevila F. Test method for boom suspension influence on spray distribution, part i: experimental study of pesticide application under a moving boom. Biosyst Eng 2007;96(1):29–39.
[5] Lardoux Y, Sinfort C, Enfalt P, Miralles A, Sevila F. Test method for boom suspension influence on spray distribution, part ii: validation and use of a spray distribution model. Biosyst Eng 2007;96(2):161–8.
[6] Karimi EP, Khajepour A, Wong A, Ansari M. Analysis and optimization of air suspension system with independent height and stiffness tuning. Int J Automot Technol 2016;17 (5):807–16.
[7] Quaglia G, Sorli M. Air suspension dimensionless analysis and design procedure. Veh Syst Dyn 2001;35(6):443–75.
[8] Alonso A, Giménez JG, Nieto J, Vinolas J. Air suspension characterization and effectiveness of a variable area orifice. Veh Syst Dyn 2010;48(sup1):271–86.
[9] Yin Y, Rakheja S, Yang J, Boileau PE. Characterization of a hydro-pneumatic suspension strut with gas-oil emulsion. Mech Syst Sig Process 2018;106:319–33.
[10] Danish A, Samuel F. Artificial intelligence models for predicting the performance of hydro-pneumatic suspension struts in large capacity dump trucks. Int J Ind Ergon 2018;67:283–95.
[11] Bittner R. Suspension system for an agricultural vehicle. U.S. Patent 8297634, 2012-10-30.
[12] Hiddema J. Agricultural application machine with variable width track. U.S. Patent 8376078, 2013-02-19.
[13] Zatrieb J, Kasler R. New generation of hydro-pneumatic suspension systems with adaptive damping, SAE Technical Paper; 2012.
[14] Carlson BC, Young DE, Baxter GE, Anderson JC. Suspended axle for sprayer. U.S. Patent 7938415, 2011-05-10.

[15] Wubben TM, Maiwald MA, Carlson BC, Anderson JC. High clearance vehicle suspension with twin spindles for transferring steering torque. U.S. Patent 7168717, 2007-01-30.
[16] Schaffer JA. Steering system for variable height agricultural sprayer. U.S. Patent 6371237, 2002-04-16.
[17] Schaffer JA. Wheel support system for agricultural sprayer. U. S. Patent 6491306, 2002-12-10.
[18] Slawson J. Independent strut suspension. U.S. Patent 8534686, 2013-09-17.
[19] Steffensen C, Michels E, Kleven JE. Suspension assemblies with bump steer control, U.S. Patent 8136824, 2012-03-20.
[20] Blaauw D. Spring-mounted spreading device. E.P. Patent 0919124, 1999-06-02.
[21] Ehlen V, Voth R. Suspension for self-propelled spreading machine. E.P. Patent 2388157, 2011-11-23.
[22] Krohn ML, Bernier KT. Self-propelled agricultural product application implement. U.S. Patent 20170311539, 2017-11-02.
[23] Čedík J, PražAn R. Comparison of tyres for self-propelled sprayers. Agron Res 2015;13(1):53–62.
[24] Tahmasebi M, Mailah M, Gohari M, Abd RR. Vibration suppression of sprayer boom structure using active torque control and iterative learning, part i: modelling and control via simulation. J Vib Control 2018;24(20):4689–99.
[25] Tahmasebi M, Gohari M, Mailah M, Abd RR. Vibration suppression of sprayer boom structure using active torque control and iterative learning, part ii: experimental implementation. J Vib Control 2018;24(20):4740–50.
[26] Tahmasebi M, Rahman RA, Mailah M, Gohari M. Roll movement control of a spray boom structure using active force control with artificial neural network strategy. J Low Freq Noise Vibr Active Control 2013;32(3):189–201.
[27] Karale DS, Kankal US, Khambalkar VP, Gajakos AV. Performance evaluation of self propelled boom sprayer. Int J Agric Eng 2014;7(1):137–41.
[28] Gao Z, Chen S, Zhao Y, Nan J. Height adjustment of vehicles based on a static equilibrium position state observation algorithm. Energies 2018;11(2):1–26.
[29] Hilgers C, Brandes J, Ilias H, Oldenettel H, Stiller A, Treder C. Active air spring suspension for greater range between adjusting for comfort and dynamic driving. Atz Worldwide 2009;111(9):12–7.
[30] Sun X, Cai Y, Yuan C, Wang S, Chen L. Vehicle height and leveling control of electronically controlled air suspension using mixed logical dynamical approach. Sci China Technol Sci 2016;59(12):1814–24.
[31] Kim H, Lee H. Fault-tolerant control algorithm for a four-corner closed-loop air suspension system. IEEE Trans Ind Electron 2011;58(10):4866–79.
[32] Kim H, Lee H. Height and leveling control of automotive air suspension system using sliding mode approach. IEEE Trans Veh Technol 2011;60(5):2027–41.
[33] Xu X, Zhou K, Zou N, Jiang H, Cui X. Hierarchical control of ride height system for electronically controlled air suspension based on variable structure and fuzzy control theory. Chinese J Mech Eng 2015;28(5):945–53.
[34] British Pacejka H. Library cataloguing in publication data. Tyre and vehicle dynamics. Elsevier; 2005. p. 483–512.
[35] Kim BS, Chi CH, Lee TK. A study on radial directional natural frequency and damping ratio in a vehicle tire. Appl Acoust 2007;68(5):538–56.